The calculation shows that the diffusion coefficient increases,

$$\Delta D \sim R/\bar{r}, \tag{19}$$

where $\bar{r}$ is the mean distance between the particles. Owing to the fact that usually $\bar{r} \gg R$, we obtain that $\Delta D \ll D$ and therefore we can neglect such an increase. Thus in this case also, the value R plays the role (but a different one) of a "critical" distance.

If the "original" electron (particle) distribution function φ_{r0}' is known, the distribution function $\eta_{r\infty}$ at a stationary excitation can be found from the following equation:

$$\frac{D}{r^2}\frac{\partial}{\partial r}\left(r^2\frac{\partial \eta_{r\infty}}{\partial r}\right)-\frac{1}{r^2}\frac{\partial}{\partial r}(r^2 u_r \eta_{r\infty}) + \frac{\kappa E}{n_\infty}\left(1+\frac{\varphi_{r0}'}{n_\infty}-\eta_{r\infty}\right)=0, \tag{20}$$

where E is the exciting intensity, κ is proportional to the absorption coefficient, n_∞ is the concentration of recombining particles, and

$$\eta_{r\infty} \to 1 \quad \text{as} \quad r \to \infty \quad \text{and} \quad \eta_{r\infty}=0 \quad \text{for} \quad r=r_0. \tag{21}$$

The magnitude p_∞ can be estimated as before from (4). On the other hand, because of the fact that in the stationary state the number of recombinations is equal to the number of ionizations, one has

$$p_\infty = \kappa E/n_\infty^2. \tag{22}$$

We can point out that contrary to (20), the formula for a nonstationary excitation becomes nonlinear.

From (20), by the way, one can obtain the following interesting result. Even for $E \to 0$ when the monomolecularity seems to be dominant, the accumulating light sum

$$n_\infty \sim \sqrt{E}. \tag{23}$$

However, such striking results (pure bimolecular accumulation) find their explanation in the fact that some part of the "congeneric" components diverges at an infinitely large distance.

Thus a problem was considered which is in some aspect more complicated (since the attraction is taken into account) than in the investigation of the temperature annihilation of radiation defects. Therefore the present paper might prove to be useful for investigators working in this field.

PHYSICAL REVIEW VOLUME 125, NUMBER 1 JANUARY 1, 1962

High-Voltage Glow Discharges in D_2 Gas. II. Cathode Fall Theory*

G. W. McClure and K. D. Granzow
Sandia Corporation, Albuquerque, New Mexico
(Received August 28, 1961)

A one-dimensional theoretical treatment of the cathode fall region of 40–100 kv glow discharges in D_2 gas is presented. The region is assumed to be fed with an external supply of slow D_2^+ ions from an adjoining plasma at one boundary and an influx of secondary electrons from a cathode forming a second boundary. As a function of the current density of plasma ions the following quantities are calculated: the energy distributions and fluxes of D^+, D_2^+, and D particles incident on the cathode, the cathode electron current, the thickness of the cathode fall region, the ratio of cathode fall electron current to plasma ion current, the potential distribution including the effect of positive-ion space charge, and the voltage vs current characteristics for a fixed cathode fall thickness. The theoretical results are compared with the experimental results of Part I. Using the available cross-section data from the literature, account is taken of D_2^+ charge exchange and dissociation, electron capture by D^+, electron loss from D, ionization of the gas by fast D^+, D_2^+, and D, and ionization by cathode secondaries. Arbitrary approximations are made to a few of the unknown cross sections.

I. INTRODUCTION

PART I[1] of this series described several diagnostic experiments on glow discharges in deuterium gas at applied potentials of 40 to 80 kv and currents of the order of 1 amp. These discharges were found to be composed of a plasma-filled region occupying about half the interelectrode space and a cathode fall region extending from the plasma to the cathode. Virtually the entire applied potential was found to appear across the cathode fall region.

Sufficient information was obtained from the analysis of the diagnostic measurements to determine the types of collision processes and modes of particle motion in both regions of the discharge. In the present paper the cathode fall region is treated theoretically in a one-dimensional approximation taking into account as fully as possible the numerous cathode fall collision processes discussed in Part I. Rigorous account is taken of the connection between the potential distribution and positive-ion space charge. The quantities derived include the energy distribution of the ions and fast neutrals incident on the cathode, the length of the cathode fall region, the potential distribution along

* Work performed under the auspices of the U. S. Atomic Energy Commission.
[1] G. W. McClure, Phys. Rev. 124, 969 (1961).

the length of the cathode fall region, and the ratio of the electron current into the plasma to the ion flow out of the plasma.

The calculations take into account charge-exchange collisions of atomic and diatomic ions with gas molecules; production of fast neutral atoms and monatomic ions by charge-exchange and dissociative collisions; ion production by collisions of electrons, ions, and fast neutral atoms with gas molecules; and secondary electron emission from the cathode due to fast ion and fast neutral atom bombardment.

Previous detailed theoretical treatments of the cathode fall region of glow discharges[2,3] pertain mainly to the so-called "normal" or "abnormal" glow discharges in which the cathode fall potential is generally in the range 0.2 to 10 kv. In this domain several of the processes listed above are completely negligible because the ion energies are relatively low. Although Neu[3] has discussed the importance of ionization by ions and the production of fast neutrals by charge exchange at higher cathode fall potentials, his mathematical theory does not properly account for either of these processes. No previous theory has included dissociation of molecular ions or electron loss from fast neutral atoms.

The primary limitations of the present theory are the following: the treatment is one dimensional, the ions from the plasma are assumed to be D_2^+ ions[4] and the fast D_2^+ ions are assumed to convert only into $D+D^+$ or $D+D$ pairs[5] (the latter by charge exchange). In spite of the questionable validity of these assumptions the theory has considerable value inasmuch as it accurately accounts for the observed cathode fall thickness, the observed energy distributions of D_2^+ and D^+ ions at the cathode, and the observed ratio of electron current to plasma ion current.

II. NATURE OF COLLISIONS AND CROSS-SECTION MAGNITUDES

The physical domain to be considered is that contained between a plane plasma surface and a plane cathode parallel to the plasma surface. A unidirectional electric field normal to both boundaries fills this space. The field will, in general, be nonuniform due to positive-ion space charge. Solutions are considered only for potentials in the range 40 to 100 kv between the boundaries.

It is assumed that the plasma region generates D_2^+ ions and that these flow into the cathode fall region uniformly from the entire plasma boundary with a negligibly small initial velocity. The subsequent acceleration of these ions toward the cathode creates (through collision processes to be discussed) complex cascades which are composed of D_2^+, D^+, D, and D_2 particles.[6] When the cascades reach their end point at the cathode, secondary electrons are released which ionize the gas and produce a volume distribution of additional D_2^+ ions. The latter also create ionic cascades which in turn release secondaries from the cathode. Only the steady state situation is considered in which all particle flows are independent of time and mutually consistent. It is assumed that the gas is composed solely of D_2 and that no significant concentration of atomic D is present.[7]

The justification for using hydrogen collision cross-section data in lieu of deuterium data has been discussed previously in Part I.

It is assumed that D_2^+ ions which diffuse across the plasma boundary start at rest and move straight toward the cathode until they undergo either charge-exchange or dissociative collisions. From the experimental results of Part I it is clear that all of the heavy particles incident on the cathode (D_2^+, D^+, D, and D_2) are essentially normally incident, hence scattering is ignored completely. Electrons released from the cathode are also assumed to undergo no scattering, also based on the results of Part I.

An accelerated D_2^+ ion or any of its cascade secondaries may, in a collision with a gas molecule, produce secondaries distinct from the primary in either of two general ways: (1) by the destruction or alteration of the primary particle itself through charge exchange or dissociation, or (2) by ionizing or dissociating a struck gas molecule. In principle, either (1) or (2) or both may occur in a single collision. The importance of distinguishing particles resulting from these two types of events lies in the fact that the secondaries from (1) conserve the velocity of the primary and have a subsequent behavior characteristic of this "initial" velocity, while secondaries from (2), which are essentially at rest immediately following a collision, cannot suffer an energetic collision until accelerated by the electric field. Because of their low kinetic energy, neutral secondaries produced in events of type (2) are ignored. Neutral secondaries from (1) cannot be ignored as these will generally have a high-kinetic energy and can therefore produce subsequent ionization by collision, release secondary electrons from the cathode, or become charged by electron loss so as to gain still more kinetic energy before arriving at the cathode.

---

[2] A. L. Ward, Phys. Rev. **112**, 1852 (1958).

[3] H. Neu, Z. Physik **155**, 77 (1959).

[4] R. N. Varney [Phys. Rev. Letters **5**, 559 (1960)] has discussed recent evidence that the principal ion species in low-temperature hydrogen plasmas is H_3^+. Presumably the corresponding species D_3^+ would issue, in addition to D_2^+, from a deuterium plasma of the type considered in part I.

[5] A. Schmid [Z. Physik **161**, 550 (1961)] has shown that fast (10–100 kev) D_2^+ ions convert partially to fast neutral molecules. The present theory does not include this effect, but the mathematical structure of the theory is well adapted to take proper account of fast D_2 production and destruction when the cross sections for the various possible collision modes of the species are known.

[6] The production of negative ions is ignored.

[7] The discharges investigated in Part I, which the present theory is to describe, probably contained no significant D concentration. This point was discussed in the Introduction to Part I.

To treat the development of the heavy-particle cascades, it is expedient to introduce a special cross-section notation with numerical subscripts to designate the primary and secondary particles involved in the collisions. The numerical subscripts 1, 2, 3, 4, 5, represented in general by the letters i or j, denote particles D_2^+, D_2, D^+, D, and e respectively, where e represents an electron. The total cross section for the destruction of a particle of type $i \neq 5$ is a_i. Such destruction always leads to the production of one or more fast secondaries through events of type (1). The partial cross section for the production of each possible species of *fast* secondary in a type-1 event is denoted f_{ij}, where i represents the primary and j the secondary. Likewise the production cross section of each possible species of *slow* secondary (event of type 2) is represented by the symbol s_{ij} where i refers to the primary and j to the secondary. Each of the cross-section symbols represents a function of the energy of the primary particle.

To illustrate the application of this specialized cross-section notation consider the possible modes of destruction of a D_2^+ ion:

$D_2^+ + e \rightarrow D_2$, reaction a, cross section σ_a,

$D_2^+ + e \rightarrow D + D$, reaction b, cross section σ_b,

$D_2^+ \rightarrow D + D^+$, reaction c, cross section σ_c,

$D_2^+ \rightarrow D^+ + D^+ + e$, reaction d, cross section σ_d.

In reactions a and b, the electron on the left is captured from the struck molecule. The relations between the reaction cross sections σ_a, σ_b, σ_c, σ_d, and the specialized cross sections defined above are:

$$a_1 = \sigma_a + \sigma_b + \sigma_c + \sigma_d,$$
$$f_{12} = \sigma_a,$$
$$f_{13} = \sigma_c + 2\sigma_d,$$
$$f_{14} = 2\sigma_b + \sigma_c.$$

Cross sections which have been measured in the energy range of interest include the so-called total charge-exchange cross section $\sigma_{ce} = \sigma_a + \sigma_b - \sigma_d$ and the cross section f_{13} (see Fig. 1[8–13]). The sum of these equals the total cross section a_1. Below 6 kev where no measurements are available, f_{13} is assumed to vary as the first power of the ion energy. As mentioned earlier, no data are available on the dissociation of the fast D_2 neutrals from reaction a. In the absence of this information it is assumed that a fast D_2 acts exactly as a pair of separate D atoms. This is implemented by setting $f_{12} = 0$ and $f_{14} = 2a_1 - f_{13}$ which ensures that the combined production of fast D and D^+ conserves the mass and energy of the destructed D_2^+.

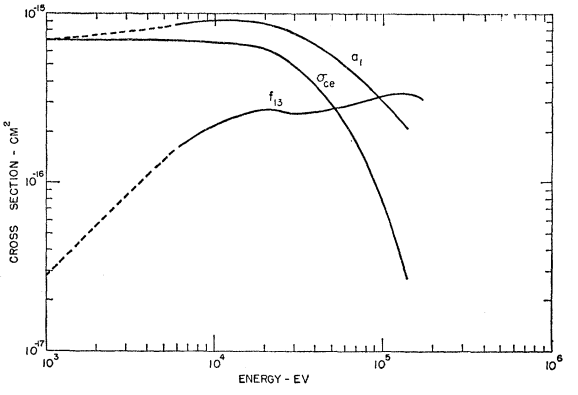

FIG. 1. Cross-section data used for the calculation of D_2^+ ion breakup. Plotted curves are for H_2^+ ions impacting on H_2 molecules; the energy values were multiplied by 2 for the deuterium calculations. σ_{ce}: charge-exchange cross section[8–11]. f_{13}: H^+ production by dissociation of H_2^+ [12–13]; a_1: destruction of H_2^+ (see text). Dashed portions of curves are extrapolations chosen by the authors.

The measured cross sections corresponding to the designations s_{11}, s_{13}, and s_{15}, are shown in Fig. 2.[14,15] Below 5 kev, where s_{13} has not been measured, it is assumed that the cross section varies as the first power of the ion energy. In the same energy range s_{11} has not been measured, but it is certain that the major part of the slow molecular ion production in this energy range results from charge exchange. (An upper limit on the cross section for slow molecular ion production by processes other than charge exchange is given by s_{15} which becomes $<10\%$ of σ_{ce} below 5 kev.) Hence, s_{11} is set equal to σ_{ce} below 5 kev.

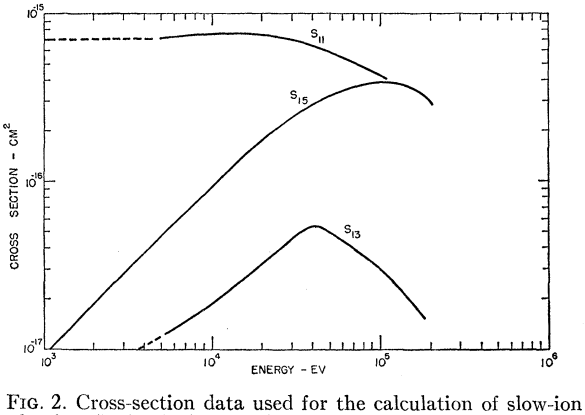

FIG. 2. Cross-section data used for the calculation of slow-ion production (ionization) by D_2^+ ions. Plotted curves are for H_2^+ ions impacting on H_2 molecules; the energy values were multiplied by 2 for the deuterium calculations. s_{11}: production of H_2^+ ions[14]; s_{13}: production of H^+ ions[14]; s_{15}: production of free electrons.[9,11,14,15] Dashed portions of curves are extrapolations chosen by the authors.

[8] J. B. H. Stedeford and J. B. Hasted, Proc. Roy. Soc. (London) **A227**, 466 (1955).
[9] J. P. Keene, Phil. Mag. **40**, 369 (1949).
[10] V. V. Afrosimov, R. N. Ilin, and N. V. Fedorenko, Soviet Phys.-JETP **34**, 968 (1958).
[11] F. Schwirtzke, Z. Physik **157**, 510 (1960).
[12] N. V. Fedorenko, V. V. Afrosimov, R. N. Ilin, and D. M. Kaminker, Soviet Phys. JETP **36**, 267 (1959).
[13] A. Schmid, Z. Physik **161**, 550 (1961).
[14] V. V. Afrosimov, R. N. Ilin, and N. V. Fedorenko, Soviet Phys. JETP **34**, 968 (1958).
[15] H. B. Gilbody and J. B. Hasted, Proc. Roy. Soc. (London) **A240**, 382 (1957).

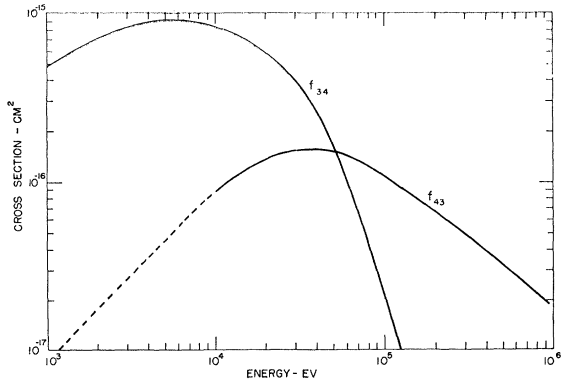

FIG. 3. Cross-section data used for the calculation of electron capture by D^+ and electron loss from D. Plotted curves are for H^+ and H impacting on H_2 gas; the energy values were multiplied by 2 for the deuterium calculations. f_{34}: electron capture by H^+ [8,9,16,17]; f_{43} electron loss from H.[11,16–19] Dashed portions of curves are extrapolations chosen by the authors.

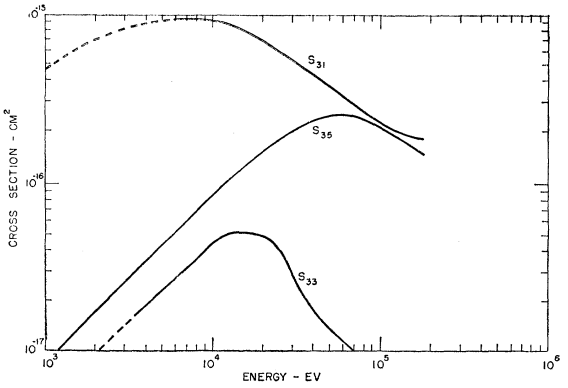

FIG. 4. Cross-section data used for the calculation of slow-ion production (ionization) by D^+ ions. Plotted curves are for H^+ ions impacting on H_2 molecules; the energy values were multiplied by 2 for the deuterium calculations. s_{31}: production of H_2^+ ions[14]; s_{33}: production of H^+ ions[14]; s_{35}: production of free electrons.[7,11,14,15,19] Dashed portions of the curves are extrapolations chosen by the authors.

The only significant process destructive of fast D^+ ions is

$$D^+ + e \rightarrow D,$$

where the electron on the left is captured from a gas molecule. The measured cross section for this purpose f_{34} is shown in Fig. 3.[16–19] Obviously, $a_3 = f_{34}$.

The only significant process destructive of fast D is the process

$$D \rightarrow D^+ + e.$$

The measured cross section for this process $f_{43} = a_4$ is shown in Fig. 3. Below 10 kev, where f_{43} has not been measured, a variation proportional to the first power of the incident D energy is assumed.

The measured cross sections s_{31}, s_{33}, and s_{35} are shown in Fig. 4. Below 6 kev, where s_{31} has not been measured, it is practically certain that $s_{31} = f_{34}$. This approximation is indicated by the dashed curve. (An upper limit to the contribution of processes other than charge exchange to s_{31} is given by s_{35} which becomes very much smaller than the charge-exchange cross section below 6 kev.)

The remaining cross sections required for the calculation are those for slow-ion production by neutral atoms (s_{41} and s_{43}) and by electrons (s_{51} and s_{53}). The former have not been measured separately, but according to Schwirtzke,[11] the total ion production cross section ($s_{41}+s_{43}$) is essentially equal to the electron loss cross section f_{43}. In the present calculations we set $s_{41} = f_{43}$ and set $s_{43} = 0$. The sum ($s_{51}+s_{53}$) has been measured by several investigators. A working cross-section curve from the available data has been plotted in Part I. According to the findings of Bleakney[20] and Newhall,[21] s_{51} is much larger than s_{53}, hence we set s_{51} equal to the measured total ionization cross section and set $s_{53} = 0$.

The curves given in Figs. 1–4 are not necessarily representative of any particular reference, but are, in the opinion of the authors, the best present estimate based on all known experimental data. In most cases the results of all authors fall within $\pm 20\%$ of the curves we have drawn.

For numerical values of the secondary emission coefficients, γ_i, of positive ions and neutrals the data obtained in Part I were used. Below the lower energy limit of these measurements (15 kev for D_2^+ and 7.5 kev of D^+) γ_i is assumed to vary as the first power of the ion energy. D neutrals are assumed to have the same secondary emission coefficients as D^+ ions of the same energy.[22]

In the present theory we ignore entirely the secondary effects produced by electrons released in gaseous collisions. With the high cathode fall potentials to be considered, the probability that an electron released anywhere within the cathode fall region will undergo an ionizing collision before entering the plasma is <0.02. Hence the ion production introduced by gas secondary electrons is negligible.

[16] P. M. Stier and C. F. Barnett, Phys. Rev. **103**, 896 (1956).
[17] F. L. Ribe, Phys. Rev. **83**, 1217 (1951).
[18] C. F. Barnett, H. K. Reynolds, and R. G. Reinhardt, Oak Ridge National Laboratory Progress Report ORNL 2204, 1956 (unpublished).
[19] I. M. Fogel, V. A. Ankudinov, D. V. Pilipenko, and N. V. Topolia, Sov. Phys. JETP **34**, 400 (1958).
[20] Walter Bleakney, Phys. Rev. **35**, 1181 (1930).
[21] H. F. Newhall, Phys. Rev. **62**, 11 (1942).
[22] The results of V. G. Telkovskii [Soviet Phys. Doklady **1**, 334 (1957)] indicate that H^+, H_2^+, and H_3^+ ions of the same velocity have secondary emission coefficients in the ratio 1:2:3, respectively. This suggests that the molecules, upon entering the metal surface, break up into separate H^+ atoms and H neutrals which act as separate and equivalent secondary electron producers. The results of Part I concerning the relative secondary emission coefficients of D^+ and D_2^+ ions also support this assumption. The results of F. Schwirtzke[11] while in conflict with the above results concerning the H^+, H_2^+, and H_3^+ species, indicate that H and H^+ have the same secondary emission coefficients, within 25%, between 10 and 60 kev.

The energy losses suffered by both ions and electrons due to ionizing collisions are completely negligible compared to the energy gain from the electric field in one ionization mean-free path. Hence the electric field is regarded as the sole factor affecting the energy of a particle from the time it is created until it is destroyed (i.e., changed to another species).

The energy attained by a D_2^+ ion before its conversion to another species is $\sim\frac{1}{5}$ the cathode fall potential; hence, very few D_2^+ ions move all the way from the plasma to the cathode without undergoing conversion to other species (see Part I). The ionization mean free paths for D^+ and D_2^+ ions and for D neutrals are of the order of the observed cathode fall length. Thus the production of slow ions by ion collisions is a first order effect.

III. MATHEMATICAL FORMULATION

The following list defines the symbols used in the equations to follow:

Index numbers 1, 2, 3, 4, 5 refer to D_2^+, D_2, D^+, D, and e, respectively.
x = distance toward cathode measured from the boundary of the plasma.
d = value of x at the cathode.
$\epsilon=\frac{1}{2}v^2$, where v is the velocity of the particle being described (ϵ is herein referred to as the "reduced energy").
ϵ_{max} appears in the equations as a limit of integration and represents the maximum value of ϵ attainable by a particle of type i in the cathode fall region. In general $\epsilon_{max}=eV_c/m_i$.
$\phi_i(\epsilon,x)d\epsilon$ = the flux of particles of type i at position x with reduced energy in the interval ϵ to $\epsilon+d\epsilon$.
$a_i(\epsilon)$ defined in Sec. II.
$f_{ij}(\epsilon)$ defined in Sec. II.
$s_{ij}(\epsilon)$ defined in Sec. II.
N = the number density of gas molecules.
m_i = mass of particle of type i.
q_i = charge of particle of type i.
$E(x)$ = electric field intensity.
$V(x)$ = electric potential relative to the plane $x=0$.
$V_c=V(d)$ = electric potential of the cathode.
e = magnitude of electronic charge.
J_A^+ = electric current density at $x=0$ due to D_2^+ ions flowing from the plasma into the cathode fall region.
J_K^+ = electric current density due to D_2^+ and D^+ ions incident on the cathode.
J^- = electric current density due to secondary electrons emitted from the cathode.
$\mu=J_A^+/J^-$, the plasma ion emission per cathode secondary electron.
$\rho_+(x)$ = electric charge density due to positive ions.
$\gamma_i(\epsilon)$ = secondary emission coefficient of particles of type i with reduced energy ϵ.
$\delta(y)$ = Dirac delta function of y.

On the basis of the assumptions discussed in Sec. II the total differential change of flux $d\phi_i$ of a particle species between x and $x+dx$ due to collisions is

$$d\phi_i(\epsilon,x)=N[\sum_{j=1}^{4} f_{ji}\phi_j-a_i\phi_i]dx;\quad i=1,2,3,4;\quad \epsilon\neq 0,$$

but since

$$\frac{d\phi_i(\epsilon,x)}{dx}=\frac{\partial\phi_i}{\partial\epsilon}\frac{d\epsilon}{dx}+\frac{\partial\phi_i}{\partial x}=\frac{q_i}{m_i}E\frac{\partial\phi_i}{\partial\epsilon}+\frac{\partial\phi_i}{\partial x},$$

the following partial differential equation is obtained:

$$\frac{\partial\phi_i}{\partial x}+\frac{q_i}{m_i}E\frac{\partial\phi_i}{\partial\epsilon}=N[\sum_{j=1}^{4} f_{ji}\phi_j-a_i\phi_i];\ i=1,2,3,4,\ \epsilon\neq 0. \quad (1)$$

The production of zero-energy ions is described by the condition

$$\begin{aligned}\phi_i(0,x)&=\frac{m_i}{q_i}\frac{N}{E}\sum_{j=1}^{5}\int_0^{\epsilon_{max}} s_{ji}\phi_j d\epsilon, && i=1,3\\ &=0, && i=2,4.\end{aligned} \quad (2)$$

The flow of D_2^+ ions from the plasma into the cathode fall region yields the boundary condition at $x=0$:

$$\begin{aligned}\phi_i(\epsilon,0)&=\delta(\epsilon)J_A^+/e, && i=1\\ &=0, && i=2,3,4.\end{aligned} \quad (3)$$

The electron flux, given in terms of the secondary emission coefficients, $\gamma_i(\epsilon)$, is

$$\phi_5(\epsilon,x)=\delta\left\{\epsilon-\frac{e}{m_5}[V(x)-V_c]\right\}\times\sum_{i=1}^{4}\int_0^{\epsilon_{max}}\gamma_i(\epsilon)\phi_i(\epsilon,d)d\epsilon. \quad (4)$$

The summation of integrals on the right equals the cathode electron current J^-. In Eqs. (1) and (2) E is given by

$$E=\int_0^x 4\pi\rho_+(x)dx=4\pi e\times\int_0^x\int_0^{\epsilon_{max}}\frac{1}{(2\epsilon)^{\frac{1}{2}}}[\phi_1(\epsilon,x)+\phi_3(\epsilon,x)]d\epsilon dx. \quad (5)$$

This implies that the electric field at the plasma surface is zero which is in accordance with the extremely small variation of the potential within the plasma observed in Part I.

In equation (4) V is given by

$$V(x)=-\int_0^x Edx. \quad (6)$$

The partial differential equation [Eq. (1)] is soluble

by numerical integration subject to the condition imposed by the subsequent equations. The quantities J_A^+ and V_c are parameters in the problem and the quantities f_{ij}, s_{ij}, and γ_i are assigned values as discussed in Sec. II. Besides the unknown functions ϕ_i, the potential distribution $V(x)$, and the length d are obtained in the solution of the problem.

The method of numerical integration used in the solution of the equations is discussed in the Appendix.

IV. NUMERICAL RESULTS

Numerical solutions of the equations were obtained (with an IBM 704 computer) for $V_c=40$, 60, 80, and 100 kv and for J_A^+ of the order of magnitude to permit comparisons of the theoretical results with the experimental results of Part I. Throughout this section the current densities J_A^+, J_K^+, J^-, and the flux densities ϕ_i are expressed in the "reduced" form J_A^+/p^2, J_K^+/p^2, J^-/p^2, and ϕ_i/p^2, respectively, where p is the pressure. The cathode fall thickness d is expressed in the "reduced" form pd. The use of these forms eliminates the pressure as an independent parameter without limiting the generality of the results.

Figure 5 is a plot of calculated values of J_K^+/p^2, pd, and μ vs J_A^+/p^2 for $V_c=80$ kv. Under the conditions of the ion spectrum measurements of Part I [$V_c=80$ kv, $J_K^+/p^2=23.8$ amp cm^{-2} (mm Hg)$^{-2}$] the theoretical curves predict $pd=0.212$ mm Hg cm and $\mu=0.0223$. The theoretical value of pd agrees within experimental error with the experimental value 0.216 ± 0.010 mm Hg cm obtained from the wall potential measurements [Eq. (3), Part I]. The precision of this agreement is somewhat surprising since the ion current at the cathode of the experimental tubes was concentrated in a small area near the center of the cathode while the plasma surface extended essentially across full tube diameter. This indicates a radial convergence of the ion flow in the experimental situation which is not exactly comparable to the parallel flow assumed in the theory. As a result of this convergence one would expect a difference in the experimental and theoretical space-charge distributions and a corresponding difference in the cathode fall thicknesses for the same cathode current densities. A possible explanation for the absence of a large discrepancy is that the ion beam in the experimental tubes converges very sharply near the plasma and then proceeds at a constant diameter throughout the major part of the cathode fall space.

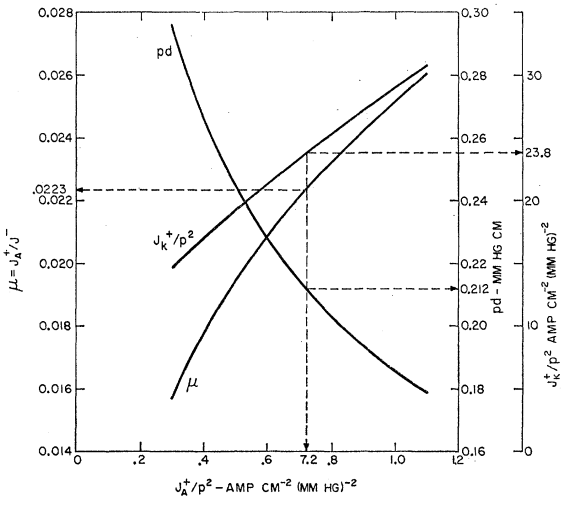

FIG. 5. Self-consistent solutions for the reduced cathode positive-ion current density (J_K^+/p^2), the reduced cathode fall thickness (pd) and the ratio of plasma ion current density to electron current density (μ) all vs the reduced plasma ion current density (J_A^+/p^2). Calculations are based on a cathode fall potential of 80 kv. For $(J_K^+/p^2)=23.8$ amp cm^{-2} (mm Hg)$^{-2}$ the theory predicts: $J_A^+/p^2=7.2$ amp cm^{-2} (mm Hg)$^{-2}$, $pd=0.212$ mm Hg cm, and $\mu=0.0223$. Dashed lines indicate the scale readings.

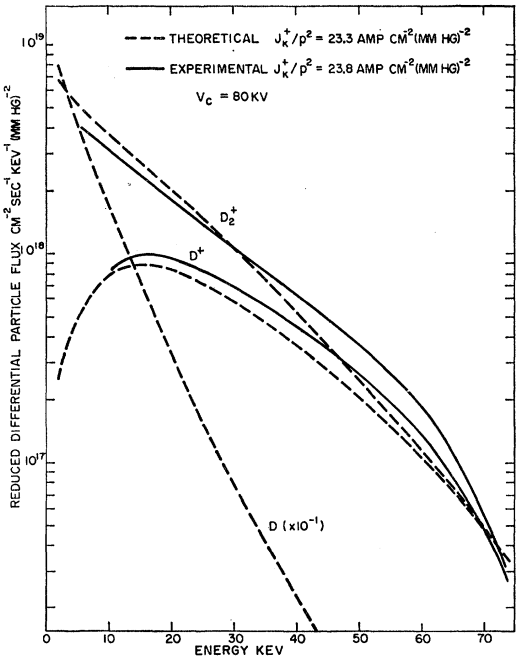

FIG. 6. Experimental and theoretical energy distributions of D_2^+ and D^+ ions incident on the cathode and theoretical spectrum of D atoms incident on cathode. Arbitrary vertical normalization of experimental data is used because the absolute differential ion fluxes were not measured. The value of J_K^+/p^2 for the theoretical curves differs slightly from the experimental value. This small difference cannot account for the discrepancies in the spectra.

In view of the departure from parallel ion flow in the experimental tubes one would expect that the ratio of plasma ion current density to cathode electron current density would be very different from the theoretical value, and in fact, a 30-fold discrepancy exists between these quantities. One would nonetheless expect on the basis of charge conservation to find the theoretical ratio μ in close agreement with the experimental ratio of plasma total current to cathode electron current [Eq. (13), Part I]. In this case, the theoretical and experimental results agree within 2%.

Figure 6 shows a comparison between the experi-

mental and theoretical ion energy spectra at the cathode. The theoretical and experimental spectra are quite similar in over-all shape, but the theoretical spectra do not have the distinct "knee" in the neighborhood of 60 kev which is evident in the experimental spectra. The shape and position of the maximum in the D^+ spectrum at 15 kev is accurately reproduced by the theory. The neutral atom spectrum given by the theory (shown reduced by a factor of 10) indicates a predominance of neutral particle flux over total ion flux below 25 kev.

In Part I the ratio of the secondary emission current due to neutrals to the total of positive-ion current plus secondary emission current due to positive ions $[I_e^0/(I^+ + I_e^+)$ in the notation used in Part I] was found to be 1.1. The value of the same quantity from the theory is 1.6. This discrepancy possibly results from the assumption of too high a secondary emission coefficient for the neutrals in the theory. If one were to lower the γ values for neutrals by an amount sufficient to remove this discrepancy, the value of μ obtained from the theory would be about 25% higher than the experimental value. In view of the uncertainties in the method used to calculate μ from the experimental results, this is not serious disagreement.

Figure 7 shows the sensitivity of the calculated ion and neutral spectra at the cathode to the value of J_K^+/p^2. These curves show that the mean energy of the ions at the cathode increases as J_K^+/p^2 increases. Such a result is to be expected, since increased current

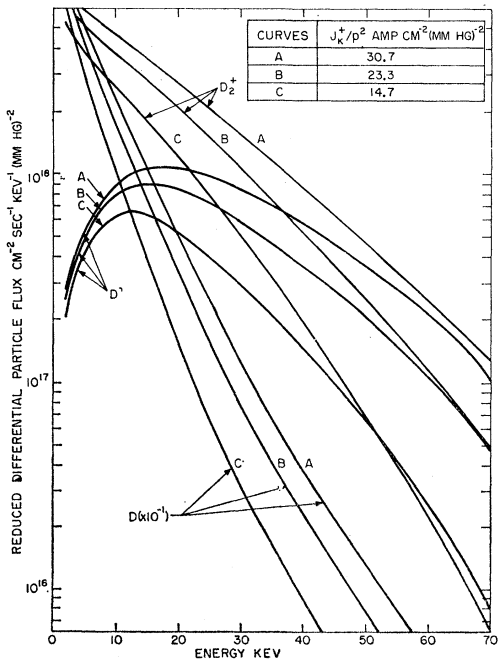

FIG. 7. Theoretical D_2^+, D^+, and D energy spectra at the cathode for various values of J_K^+/p^2 neighboring the value 23.3 amp cm^{-2} (mm Hg)$^{-2}$ for which data are shown in Fig. 6.

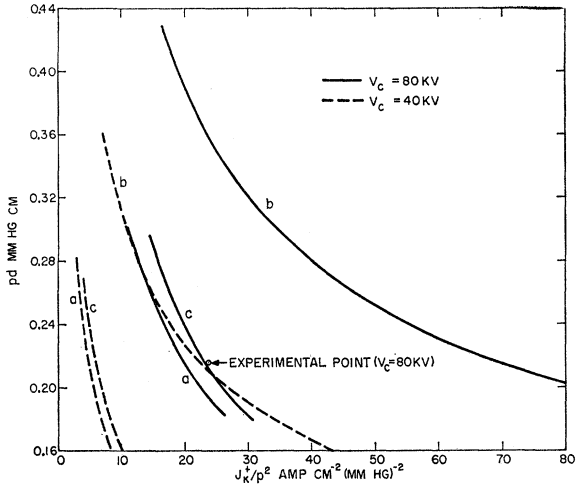

FIG. 8. Theoretical reduced cathode fall thickness (pd) vs reduced cathode current density (J_K^+/p^2) for the cases: (a) uniform current density of D_2^+ ions from plasma, but no cathode electron emission, (b) cathode secondary emission but no ion current into cathode fall from plasma, (c) self-consistent solution including both plasma ion current and cathode secondary emission.

density leads to a smaller value of pd (see Fig. 5) and a correspondingly smaller ion collision probability in the cathode fall.

To ascertain the relative effect on pd of ions fed from the plasma into the cathode fall and ions produced in the cathode fall by cathode secondary electrons, calculations were made for $V_c = 40$ and 80 kv omitting first one source of ions and then the other. The results are shown in Fig. 8. The middle 80-kv curve, which represents the self-consistent solution (both sources of ions included), is in much better agreement with the experimental point plotted than either of the two special solutions. The relatively small effect on pd of eliminating ionization due to cathode secondaries arises from the fact that most of the space charge in the self-consistent solution comes from the ions emitted by the plasma and from the ionization secondaries of these ions.

By trial and error variation of J_A^+/p^2, self-consistent solutions were obtained for $V_c = 100$, 80, 60, and 40 kv corresponding to the observed cathode fall length of 0.216 mm Hg-cm. A log-log graphical plot of the cathode current density $(J^- + J_K^+)/p^2$ vs V_c showed that to a very precise approximation $(J^- + J_K^+)$ was proportional to the 2.34 power of V_c. For the discharges investigated in Part I, the exponent of the *total* current vs voltage dependence was 2.9. Variations in the cross-sectional area of the ion beam in the experimental tube could conceivably account for the discrepancy between the theoretical current density behavior as compared with the experimental total current behavior.

The function $V(x)$ was plotted on a log-log graph for the case $V_c = 80$ kv and $J_K^+/p^2 = 23.3$ amp cm^{-2} (mm Hg)$^{-2}$. The plot was found to be represented by

the analytic function

$$V(x)=V_c(x/d)^{1.65},$$

within 2% accuracy over the range $4<V<80$ kv. A comparison of this function with the cathode fall wall potential distribution measured in Part I for $V_c=80$ kv, indicates that the walls are everywhere at a more positive potential than the theoretical space potential. This provides a semi-empirical explanation for the focusing of the ion current toward the central axis of the tube. The reason for a wall potential in excess of the amount required to merely keep the ions from hitting the walls is not yet clear. It is possible that the positive "overcharging" occurred during the formative phase of the experimental discharge and that the excess charge did not have time to leak off during the short ($<100\,\mu$sec) periods during which the observations were made.

V. CONCLUSIONS

The excellent correlation between the experimental results of Part I and the theory herein presented leads the authors to believe that the proposed theoretical model encompasses rather completely the basic processes occurring in the cathode fall region of a high-voltage D_2 glow discharge. The chief shortcomings of the theory include: (1) the assumption that the ions from the plasma are of the D_2^+ species when in fact strong indirect evidence exists that the predominant ion is D_3^+, (2) the oversimplified method of dealing with dissociation of fast D_2 molecules, and (3) the assumption of uniform and unidirectional (parallel) ion flow. The mathematical methods here introduced are easily extendable to include proper treatment of D_3^+ and fast D_2 when the cross sections for the various possible modes of destruction of these species are known. To attempt a full three-dimensional solution of the problem including the effects of wall charges would be a most formidable undertaking. It is doubtful that such a treatment would add much in the way of useful physical insight.

ACKNOWLEDGMENTS

C. J. MacCallum and R. S. Berner contributed much to this investigation by performing preliminary calculations on simpler versions of the problem.

APPENDIX

The numerical solution of Eq. (1) is accomplished by a stepwise numerical integration. The cathode fall region is divided into a prescribed number of equipotential increments. Suppose that at the point x, $\phi_i(\epsilon,x)$, $V(x)$, and $E(x)$ are known from prior calculation. The next step is to find $\phi_i(\epsilon, x+\Delta x)$, $E(x+\Delta x)$, and Δx for the next interval (in which ΔV has a preset value). The sub-steps used to accomplish this follow:

1. The energy of the fluxes of charged particles is increased by one increment. This is accomplished merely by a shift in memory location. It yields the particle spectra at $x+\Delta x$ supposing all cross sections equal to zero.

2. Using Eq. (5), both the interval length, Δx, and the electric field at $x+\Delta x$ are calculated. In this calculation, the charge density is considered constant throughout the interval and equal to the charge density produced by the fluxes calculated in sub-step (1).

3. The change in the fluxes of the various particle species is then calculated and used to augment the results of substep (1). The change in the fast-particle fluxes in the increment is merely the right side of Eq. (1) multiplied by Δx and evaluated for each energy. The flux of zero-energy particles formed in the increment, given by Eq. (2), is evaluated and stored in the lowest energy memory locations left vacant by the shift described in substep (1). [When the integral in Eq. (2) is considered a numerical sum, the expression simplifies since $\Delta\epsilon=\Delta x q_i E/m_i$.]

A typical calculation proceeds in the following way. A value of J_A^+ and V_c (parameters of the problem) are chosen. The number of potential increments to be used is chosen. An "educated guess" of J^- is made. The three sub-steps outlined above are repeated starting at $V=0$ (and $x=0$) and proceeding until $V=V_c$. Then J^- is calculated using the secondary emission coefficients and cathode ion fluxes [Eq. (4)]. The calculated J^- is compared to the assumed J^-; a correction is made in the assumed value and the whole process is repeated until self-consistency is obtained. About 3 repetitions yielded 0.1% agreement between the assumed and calculated values of J^-.

The computer program was written so that the number of potential increments could be varied from 40 to 240. Preliminary computer runs showed that 160 increments provided ample precision for the present purposes. Typical solutions for a given set of values of J^-, J_A^+, and V_c required about 12 minutes on the IBM 704. The cross-section data and secondary emission coefficients were fed to the machine in the form of tables and a linear interpolation scheme was used to find values from the tables.